Self-shading correction for oceanographic upwelling radiometers

Robert A. Leathers, Trijntje Valerie Downes

Optical Sciences Division, U. S. Naval Research Laboratory
4555 Overlook Avenue SW, Washington, DC 20375
leathers@nrl.navy.mil, downes@nrl.navy.mil

Curtis D. Mobley

Sequoia Scientific, 2700 Richards Road, Suite 107, Bellevue, Washington 98005
mobley@sequoiasci.com

Abstract: We present the derivation of an analytical model for the self-shading error of an oceanographic upwelling radiometer. The radiometer is assumed to be cylindrical and can either be a profiling instrument or include a wider cylindrical buoy for floating at the sea surface. The model treats both optically shallow and optically deep water conditions and can be applied any distance off the seafloor. We evaluate the model by comparing its results to those from Monte Carlo simulations. The analytical model performs well over a large range of environmental conditions and provides a significant improvement to previous analytical models. The model is intended for investigators who need to apply self-shading corrections to radiometer data but who do not have the ability to compute shading corrections with Monte Carlo simulations. The model also can provide guidance for instrument design and cruise planning.

©2004 Optical Society of America

OCIS codes: (010.4450) Ocean Optics; (290.4210) Multiple Scattering

References and links

1. H. R. Gordon and K. Ding, "Self-shading of in-water optical instruments," Limnol. Oceanogr. **37**, 491-500 (1992).
2. R. A. Leathers, T. V. Downes, and C. D. Mobley, "Self-shading correction for upwelling sea-surface radiance measurements made with buoyed instruments," Opt. Express **8**, 561-570 (2001).
3. D. R. Lyzenga, "Remote sensing of bottom reflectance and water attenuation parameters in shallow water using aircraft and Landsat data," Int. J. Remote Sensing **2**, 71-82 (1981).
4. J. E. O'Reilley, S. Maritorena, B. G. Mitchell, D. A. Siegel, K. L. Carder, S. A. Garver, M. Kahru, and C. McClain, "Ocean color chlorophyll algorithms for SeaWiFS," J. Geophys. Res. **103**, 24937-24953 (1998).
5. E. M. Louchard, R. P. Reid, C. F. Stephens, C. O. Davis, R. A. Leathers, T. V. Downes, and R. Maffione, "Derivative analysis of absorption features in hyperspectral remote sensing data of carbonate sediments," Opt. Express **10**, 1573-1584 (2002).
6. E. M. Louchard, R. P. Reid, F. C. Stephens, C. O. Davis, R. A. Leathers, and T. V. Downes, "Optical remote sensing of benthic habitats and bathymetry in coastal environments at Lee Stocking Island, Bahamas: A comparative spectral classification approach," Limnol. Oceanogr. **48**, 511-521 (2003).
7. H. M. Dierssen, R. C. Zimmerman, R. A. Leathers, T. V. Downes, and C. O. Davis, "Ocean color remote sensing of seagrass and bathymetry in the Bahamas Banks by high-resolution airborne imagery," Limnol. Oceanogr. **48**, 444-455 (2003).
8. J. L. Mueller et al., "Ocean optics protocols for satellite ocean color sensor validation, Revision 4, Volume III: radiometric measurements and data analysis protocols," National Aeronautical and Space Administration Report 21621 (2003).
9. G. Zibordi and G. M. Ferrari, "Instrument self-shading in underwater optical measurements: experimental data," Appl. Opt. **34**, 2750-2754 (1995).
10. E. Aas and B. Korsbø, "Self-shading effect by radiance meters on upward radiance observed in coastal waters," Limnol. Oceanogr. **42**, 974-980 (1997).
11. J. Piskozub, A. R. Weeks, J. N. Schwarz, and I. S. Robinson, "Self-shading of upwelling irradiance for an instrument with sensors on a sidearm," Appl. Opt. **39**, 1872-1878 (2000).

#5125 - $15.00 US Received 25 August 2004; revised 15 September 2004; accepted 16 September 2004

12. C. D. Mobley, *Light and Water* (Academic Press, New York, 1994).
13. R. A. Leathers and N. J. McCormick, "Algorithms for ocean-bottom albedo determination from in-water natural-light measurements," Appl. Opt. **38**, 3199-3205 (1999).
14. K. S. Baker and R. C. Smith, "Irradiance transmittance through the air-water interface," in Ocean Optics X, R. W. Spinrad, ed., Proc. SPIE **1302**, 556-565 (1990).
15. J. Piskozub, "Effects of surface waves and sea-bottom on self-shading on in-water optical instruments," in Ocean Optics XII, J. Jaffe, ed., Proc. SPIE **2258**, 300-308 (1994).

1. Introduction

When a radiometer is positioned to measure upwelling light, its shadow decreases the magnitude of the local light field, causing measured values of upwelling radiance, and hence remote sensing reflectance, to be too low. The magnitude of the error depends on wavelength, sensor size, water turbidity, and illumination conditions [1], and in shallow water it also depends on the water depth and seafloor reflectivity [2]. The self-shading error has a direct effect on the measurement of atmospheric optical thickness and on remote sensing sensor calibration. Furthermore, because the magnitude of the shading error is wavelength dependent, algorithms that depend on the spectral shape of upwelling radiance to determine water properties, water depth, or water characteristics [3–7] will also return erroneous results. Therefore, proper ocean optics protocols dictate that shading corrections should be routinely applied to all in situ upwelling light measurements [8]. Unfortunately, instrument manufacturers do not typically provide self-shading correction algorithms for their products.

We developed a Monte Carlo code [2] to compute the self-shading of buoyed radiometer data collected in 1999 and 2000 at Lee Stocking Island (LSI), Bahamas [5–7]. The self-shading of upwelling radiometers has also been investigated by other researchers [1, 9–11]; however, none of these investigations consider optically shallow waters such as those at LSI nor do they account for the additional shading caused by a flotation buoy such as that on the Hyper-TSRB.

The objective of this paper is to present a new analytical self-shading correction model for buoyed and unbuoyed upwelling radiometers. We evaluate the model with numerical simulations and then discuss the model's uses and limitations. Although Monte Carlo computations provide a more accurate method for making self-shading corrections, we believe that analytical or semianalytical models are more likely to be implemented by the general community because of the ease of which they can be disseminated and applied.

2. Model derivation

We present separate analytical shading corrections for a sensor optically far from the seafloor and a sensor close to the seafloor and then combine the two into one general correction algorithm. We derive the shading correction for a radiometer far from the seafloor by considering the idealized model shown in Fig. 1, which is a slightly generalized version of the model used by Gordon and Ding [1]. A small sensor with infinitesimally small field of view (FOV) is positioned at a distance z_s below a shading disk of radius r. The shading disk can represent the bottom of either the sensor head (if $z_s = 0$) or a buoy (if $z_s > 0$). The solar illumination is taken to be collimated and the amount of in-water scattering by water is assumed to be small enough to not significantly disturb the collimated nature of downwelling light. The goal is to determine how much the measured upwelling radiance is reduced by the shadow that falls across the sensor's line of sight.

The depth to which the shadow lies across the sensor's line of sight is [1]

$$z_0 = r/\tan\theta_{0w}\,, \tag{1}$$

where the in-water solar zenith angle θ_{0w} is related to the above-water solar zenith angle θ_0 by [12]

$$\theta_{0w} = \sin^{-1}\left(\sin\theta_0/1.338\right). \tag{2}$$

#5125 - $15.00 US Received 25 August 2004; revised 15 September 2004; accepted 16 September 2004
(C) 2004 OSA

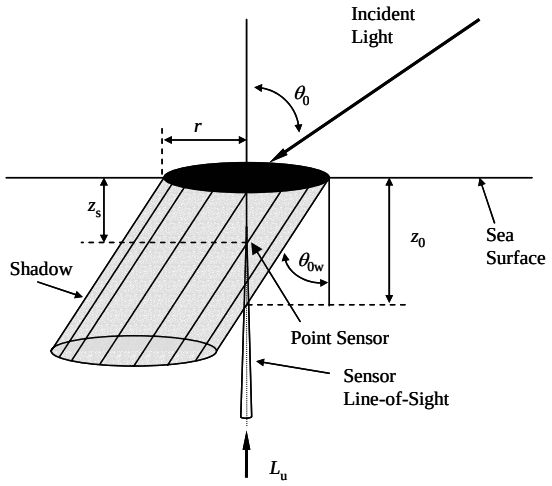

Fig. 1. Shading of an upwelling radiance sensor by a horizontal disk of radius r.

The depth dependence of the true (i.e., unshaded) radiance $L_u{}^t$ can be expressed as

$$L_u{}^t(z) = L_u{}^t(z_s)\exp\left[-K_u(z - z_s)\right], \tag{3}$$

where K_u is a depth-averaged value of the diffuse attenuation coefficient for $L_u(z)$. Because a negligible amount of light is scattered into the detector from within the shaded region, the measured radiance $L_u{}^m$ is equal to the radiance at depth z_0 attenuated back up to the sensor depth z_s,

$$L_u{}^m = L_u{}^t(z_0)\exp\left[-a(z_0 - z_s)\right]. \tag{4}$$

Using Eq. (3) to obtain $L_u{}^t(z_0)$ and substituting this into Eq. (4), we obtain

$$L_u{}^m = L_u{}^t(z_s)\exp\left[-(K_u + a)(z_0 - z_s)\right]. \tag{5}$$

For collimated light, $K_u \cong a/\cos\theta_{0w}$; substituting this and Eq. (1) into Eq. (5) gives

$$L_u{}^m = L_u{}^t(z_s)\exp\left[-k\ a(r - z_s\tan\theta_{0w})\right], \quad \tan\theta_{0w} < r/z_s\ , \tag{6}$$

where

$$k = \left(1/\tan\theta_{0w} + 1/\sin\theta_{0w}\right). \tag{7}$$

The fractional shading error in deep water is

$$\varepsilon_w = 1 - \frac{L_u{}^m}{L_u{}^t(z_s)} = \begin{Bmatrix} 1 - \exp\left[-k\ a(r - z_s\tan\theta_{0w})\right], & \tan\theta_{0w} < r/z_s \\ 0, & \tan\theta_{0w} > r/z_s \end{Bmatrix}. \tag{8}$$

For self-shading of a sensor head only (i.e., $z_s = 0$), Eq. (8) reduces to

$$\varepsilon_w = \left[1 - \exp(-k\,a\,r)\right]. \tag{9}$$

Equation (9) is the same expression derived by Gordon and Ding [1] except that they derived it using the approximation $K_u = a$ (instead of $K_u = a/\cos\theta_{0w}$), which leads to $k = 2/\tan\theta_{0w}$. The difference between $k = 2/\tan\theta_{0w}$ and $k = (1/\tan\theta_{0w} + 1/\sin\theta_{0w})$ is only significant for large values of θ_{0w}.

In our low-scattering model, the shading due to the sensor head and that due to the buoy are never additive. At small solar zenith angles, the depth of the buoy's shadow below the sensor is deeper than the depth of the sensor-head's shadow, and the sensor head contributes no shading beyond that already caused by the buoy. Conversely, the presence of the buoy contributes no additional shading to that caused by the sensor head at large solar zenith angles. The transition is at $\tan\theta_{0w} = (r_s - r_b)/z_s$, where r_s and r_b are the radii of the buoy and

#5125 - $15.00 US Received 25 August 2004; revised 15 September 2004; accepted 16 September 2004
(C) 2004 OSA

sensor head, respectively, and z_s is the distance between the bottoms of the two. The total shading of a buoyed radiometer is then simply the larger of the two effects,

$$\varepsilon_w = \begin{Bmatrix} 1-\exp\left[-k\,a\left(r_b - z_s \tan\theta_{0w}\right)\right], & \tan\theta_{0w} < \left(r_s - r_b\right)/z_s \\ 1-\exp\left[-k\,a\,r_s\right], & \tan\theta_{0w} > \left(r_s - r_b\right)/z_s \end{Bmatrix}. \qquad (10)$$

Although Fig. 1 shows the shading disk at the sea surface, Eq. (10) is valid for submerged instruments if the illumination is handled correctly; this is discussed below. Also note that the derivation of Eq. (10) assumes that the total water depth z_{bot} is greater than the depth z_0; otherwise, $\varepsilon_w = 1$.

An expression for self-shading close to the seafloor (i.e., when the upwelling light is due primarily to bottom reflection) can be developed using the model shown in Fig. 2. A sensor with finite FOV is located at depth z_s and a shading disk of radius r_d is located at depth z_d. (For the case of self-shading of the sensor head, $z_d = z_s$.) The total water depth is z_{bot}. If the seafloor is horizontal then both the sensor FOV and the shading disk project circles onto the seafloor. For a Lambertian seafloor and a sensor that responds equally to light from all directions within its FOV, the percent shading due to the shadow on the seafloor approximately equals the fraction of the FOV circle that is overlapped by the shading circle. One of four situations exists: the two circles do not overlap; the FOV circle is completely inside the shade circle; the shade circle is completely inside the FOV circle; or the two circles partially overlap. Let the x-axis lie in the horizontal plane such that the positive-x direction is looking away from the sun. The shadow on the seafloor is of radius r_d and is centered at $x_d = (\tan\theta_{0w})(z_{bot} - z_d)$. The FOV on the seafloor is centered at $x = 0$ and has radius $r_{fov} = (\tan\theta_{fov})(z_{bot} - z_s)$, where θ_{fov} is the FOV half-angle. The fractional shading can be expressed mathematically as

$$\varepsilon_B = \begin{Bmatrix} 0, & \left(x_d - r_d\right) > r_{fov} \\ 1, & \left(-r_{fov}\right) > \left(x_d - r_d\right) \\ \left(r_d / r_{fov}\right)^2, & \left(x_d + r_d\right) < r_{fov} \\ \dfrac{2}{\pi r_{fov}^2}\left(\displaystyle\int_{x_d - r_d}^{x_{int}} \sqrt{r_d^2 - \left(x - x_d\right)^2}\,dx + \int_{x_{int}}^{r_{fov}} \sqrt{r_{fov}^2 - x^2}\,dx \right), & \begin{Bmatrix} \left(-r_{fov}\right) < \left(x_d - r_d\right) < r_{fov} \\ \text{and } r_{fov} < \left(x_d + r_d\right) \end{Bmatrix} \end{Bmatrix}, \qquad (11)$$

where

$$x_d = \tan\theta_{0w}\,(z_{bot} - z_d)\,, \quad r_{fov} = [\tan\theta_{fov}\,(z_{bot} - z_s)], \quad \text{and} \quad x_{int} = \frac{r_{fov}^2 - r_d^2 + x_d^2}{2x_d}.$$

The integrals in Eq. (11) can be evaluated analytically:

$$\int_{x_d - r_d}^{x_{int}} \sqrt{r_d^2 - \left(x - x_d\right)^2}\,dx = \frac{x_{int} - x_d}{2}\sqrt{r_d^2 - \left(x_{int} - x_d\right)^2} + \frac{r_d^2}{2}\sin^{-1}\left(\frac{x_{int} - x_d}{r_d}\right) + \frac{\pi r_d^2}{4}$$

and

$$\int_{x_{int}}^{r_{fov}} \sqrt{r_{fov}^2 - x^2}\,dx = \frac{\pi r_{fov}^2}{4} - \frac{x_{int}}{2}\sqrt{r_{fov}^2 - x_{int}^2} - \frac{r_{fov}^2}{2}\sin^{-1}\left(\frac{x_{int}}{r_{fov}}\right).$$

For a buoyed radiometer, we will approximate the overall shading error close to the seafloor with

$$\varepsilon_B = \max(\varepsilon_s\,,\ \varepsilon_b), \qquad (12)$$

where ε_s is obtained from Eq. (11) with r_d and z_d taken to be the radius and depth of the sensor head and ε_b is obtained from Eq. (11) with r_d and z_d taken to be the radius and depth of the buoy.

#5125 - $15.00 US Received 25 August 2004; revised 15 September 2004; accepted 16 September 2004
(C) 2004 OSA

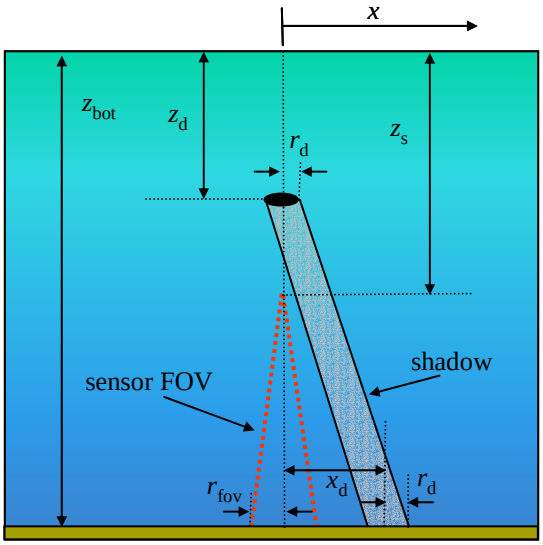

Fig. 2. Model for computing the amount of the overlap between the shadow on the seafloor and the sensor FOV.

Now that we have developed a shading model for a radiometer far from the seafloor [Eq. (10)] and a shading model for a radiometer very close to the seafloor [Eqs. (11) and (12)], the final step is to construct a transition from one to the other. We take the overall fractional error ε to be the weighted sum of the two models based on the relative importance of the signal from the seafloor at the depth of the radiometer, i.e.

$$\varepsilon = \left(\frac{L_{uw}(z_s)}{L_u^{\,t}(z_s)} \right) \varepsilon_w + \left(\frac{L_{uB}(z_s)}{L_u^{\,t}(z_s)} \right) \varepsilon_B \,, \tag{13}$$

where ε_w is obtained with Eq. (10), ε_B is obtained with Eq. (12), L_{uw} is the portion of $L_u^{\,t}$ that originates from scattering within the water column and L_{uB} is the portion of $L_u^{\,t}$ that originates at the seafloor ($L_{uB} + L_{uw} = L_u^{\,t}$). The ratios ($L_{uw}/ L_u^{\,t}$) and ($L_{uB} / L_u^{\,t}$) can be computed with a numerical radiative transfer code such as Hydrolight (Sequoia Scientific, Bellevue, Washington). Alternatively, ($L_{uw}/ L_u^{\,t}$) and ($L_{uB} / L_u^{\,t}$) can be approximated with

$$\frac{L_{uw}(z_s)}{L_u^{\,t}(z_s)} = \frac{b_b \left\{ 1 - \exp\left[-a\, \chi\, z_d \right] \right\}}{b_b + \left(R_b\, a\, \mu_{0w}\, \chi - b_b \right) \exp[-a\, \chi\, z_d]} \,, \tag{14}$$

where $z_d = z_{bot} - z_s$, $\chi = (1+1/\mu_{0w})$, and R_b is the seafloor albedo ($0 < R_b < 1$). Our derivation of Eq. (14) has been omitted for the sake of brevity. The value of R_b can be chosen either by selecting the appropriate value from published bottom reflectance spectra [6] or by esimating its value from a model of the measured light field [13].

In summary, the total error for a given incident illumination direction is given by Eq. (13), where ε_w is given by Eq. (10), ε_B is given by Eqs. (11) and (12), and the ratios $L_{uw}/L_u^{\,t}$ and $L_{uB}/L_u^{\,t}$ are either computed with a radiative transfer code or approximated with Eq. (14).

Equations (10) and (11) were derived for collimated illumination and low in-water scattering. However, these equations can be applied to more general and realistic conditions by computing a weighted average of the shading errors due to light incident on the instrument from various directions, i.e.,

$$\varepsilon = \sum_i w_i \varepsilon_i \,, \tag{15}$$

#5125 - $15.00 US Received 25 August 2004; revised 15 September 2004; accepted 16 September 2004
(C) 2004 OSA

where the weight w_i of each angular bin is proportional to the power of light incident at that directional bin. As a special case of this approach, Gordon and Ding [1] proposed taking the total shading error to be

$$\varepsilon = \varepsilon_{sky} f + (1 - f)\, \varepsilon_{sun}, \tag{16}$$

where ε_{sun} is the shading error computed for direct sunlight, ε_{sky} is the shading error of diffuse skylight, and f is the fraction of the total downwelling irradiance that is skylight. Numerically, the diffuse skylight error is approximately equal to that for direct sunlight at $\theta_0 = 35^o$ [1]. Alternatively, values of f can be computed with a radiative transfer code, such as Hydrolight. Example values of f for use in Eq. (16) are provided by Baker and Smith [14]. For a submerged instrument it may also be necessary to account for in-water scattering when estimating the angular distribution of light incident on the instrument. Furthermore, in optically shallow waters it might be necessary to account for internal reflection at the sea surface. In the last two cases, one should estimate θ_{0w} directly for use in Eqs. (10) and (11) rather than with Eq. (2).

3. Assessment

Gordon and Ding [1] used Monte Carlo simulations to develop a semi-analytical model for the self-shading of a cylindrical radiometer far from the seafloor. This model, which we will hereafter refer to as the GD model, is simply Eq. (9) with the value of k replaced with a value determined empirically from their Monte Carlo results. This value of k depends on the illumination conditions and on the size and angular response of the sensor. The GD model was verified in field experiments by Zibordi and Ferrari [9] and by Aas and Korsbø [10] and is endorsed by the ocean optics protocols for SeaWiFS validation [8]. We therefore use this as a starting point for evaluation of our more general analytical model. Table 1 shows values of k obtained three different ways: with $k = 2/\tan\theta_{0w}$ (as derived analytically by Gordon and Ding [1]), with our analytical result of $k = (1/\tan\theta_{0w} + 1/\sin\theta_{0w})$, and from the empirically derived values of the GD model for a point sensor. The values $k = (1/\tan\theta_{0w} + 1/\sin\theta_{0w})$ agree with the numerical results better than do $k = 2/\tan\theta_{0w}$, especially at large solar zenith angles. It seems likely that the difference between the GD values of k for a point source and $k = (1/\tan\theta_{0w} + 1/\sin\theta_{0w})$ is due primarily to the uncertainty in their Monte Carlo results. This assertion is based on the fact that the numerical values are slightly larger than the analytical values, whereas we would expect the opposite because the analytical model ignores the effects of scattering. In any case, our analytical values of k lie in between those of the GD model for a point sensor and those for a finite sensor (not shown in Table 1) and therefore provide a good general-purpose model for the self-shading of a unbuoyed radiometer far from the seafloor.

Table 1. Values of k [Eq. (9)] for a radiance point sensor

θ_0 (deg)	$k = 2/\tan\theta_{0w}$	$k = (1/\tan\theta_{0w} + 1/\sin\theta_{0w})$	k from numerical simulations [1]
10	15.28	15.35	16.58
20	7.56	7.69	8.43
30	4.96	5.16	5.54
40	3.65	3.91	4.18
50	2.86	3.18	3.39
60	2.36	2.72	2.84
70	2.03	2.44	2.48

Our assessment of the rest of our analytical model was performed with simulations from the backward Monte Carlo program described in Leathers et al. [2]. Many of our numerical

#5125 - $15.00 US Received 25 August 2004; revised 15 September 2004; accepted 16 September 2004
(C) 2004 OSA

computations were done with the Hyper-TSRB in mind. The Hyper-TSRB measures above-water downwelling irradiance (E_d) and underwater upwelling radiance (L_u) at many spectral channels from 400-800 nm, from which remote sensing reflectance spectra can be computed. The upwelling radiance sensor has a radius of 0.045 m and is suspended 0.66 m below the sea-surface. The buoy has a diameter of 0.15 m, and the bottom of the buoy sits 0.12 m below the sea surface and 0.54 m above the upwelling radiance sensor. The angular response of the radiance sensor was provided by Satlantic; the effective FOV is approximately 8.5 deg.

Shown in Figs. 3 and 4 is the self-shading error for the Hyper-TSRB in optically deep water predicted by Eq. (10) and for the sensor head only predicted by Eq. (9). Also shown in Figs. 3 and 4 are values of Hyper-TSRB self-shading error computed with Monte Carlo simulations for $b/a = 1$. It can be seen that the buoy adds a significant amount of shading for solar zenith angles less than 15º but contributes no additional shading beyond that of the sensor head for $\theta_0 > 15º$. Our analytical model gives excellent agreement with the numerical results in all cases except for the combination of small solar zenith angle and high water scattering. (Note that in Figs. 3 and 4 the value of b is large when a is large.) This gives us great confidence in our analytical model for most practical purposes. It should be noted that the case of $\theta_0 < 15º$ is not common except near the equator; more importantly, the actual shading error is so large for the combination of small θ_0 and high water turbidity that measurements should not be collected at these times.

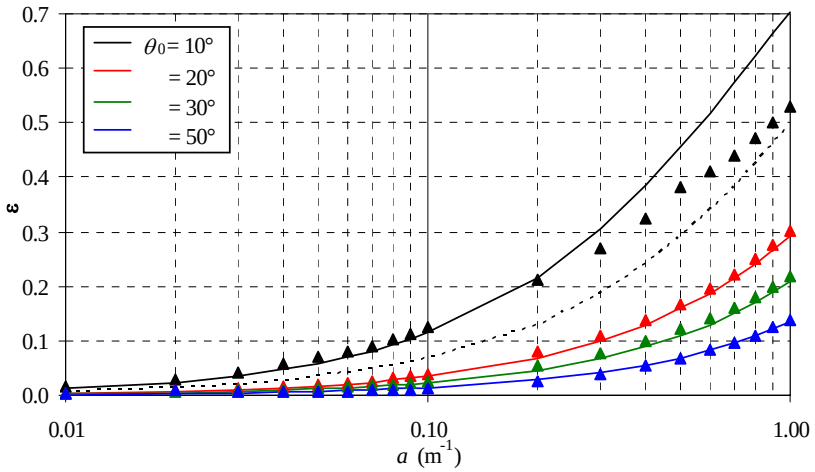

Fig. 3. Predictions of Hyper-TSRB self-shading in deep water versus water absorption: Monte Carlo calculations (triangles); analytical model for the Hyper-TSRB (solid line); and analytical model for the sensor head only (dashed lines). Error values are for direct sunlight from the solar zenith angles indicated. Analytical values assume negligible scattering; numerical results are for $b = a$.

Primarily for academic purposes we note that the disagreement between theory and numerical result at small solar zenith angle in Figs. 3 and 4 is due to the presence of scattering in the numerical simulations. The numerical results converge toward the theoretical values if the amount of scattering is decreased toward zero. As demonstrated by Gordon and Ding [1], scattering does not have a large effect on the self-shading of a unbuoyed radiometer. However, the contribution of the buoy to shading (which is primarily at small solar zenith angles) does depend significantly on the amount of scattering present since the buoy is separated by a fixed geometric distance away from the sensor. The dependence on scattering of Hyper-TSRB self-shading in optically deep water was quantified numerically by Leathers et al. [2]. It is possible to use such numerical results to make a semianalytical model for a

#5125 - $15.00 US Received 25 August 2004; revised 15 September 2004; accepted 16 September 2004
(C) 2004 OSA

particular instrument that includes the effects of scattering. For example, we can develop a semi-analytical model that accounts for scattering in deep water as follows. From Eq. (10),

$$\varepsilon = 1 - \exp\left[-\left(1 + 1/\cos\theta_{0w}\right) a \left(z_0 - z_s\right)\right], \tag{17}$$

where z_0 is given by Eq. (1). Because the depth of the shadow is reduced by scattering, we can replace z_0 in Eq. (17) with the reduced shade depth

$$z_0' = r_d \exp\left(-k_1 b z_0\right), \tag{18}$$

where r_d is the radius of the shading disk (sensor head or buoy). Shown in Fig. 5 is the self-shading error versus scattering coefficient as computed with Eqs. (17) and (18) with $k_1 = 0.1$. This provides a good model for the shading of the Hyper-TSRB in optically deep water; however, to apply this model to another buoyed instrument it would be necessary to compute a new value of k_1.

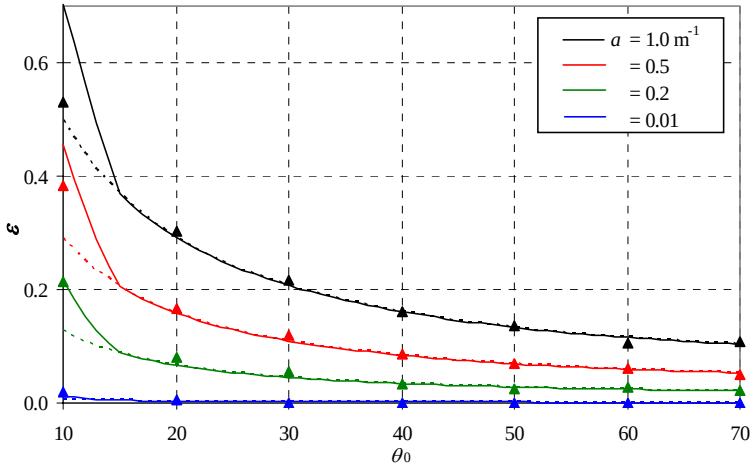

Fig. 4. Predictions of Hyper-TSRB self-shading in deep water versus sun position: Monte Carlo calculations (triangles); analytical model for the Hyper-TSRB (solid line); and analytical model for the sensor head only (dashed lines). Analytical values assume negligible scattering; numerical results are for $b = a$.

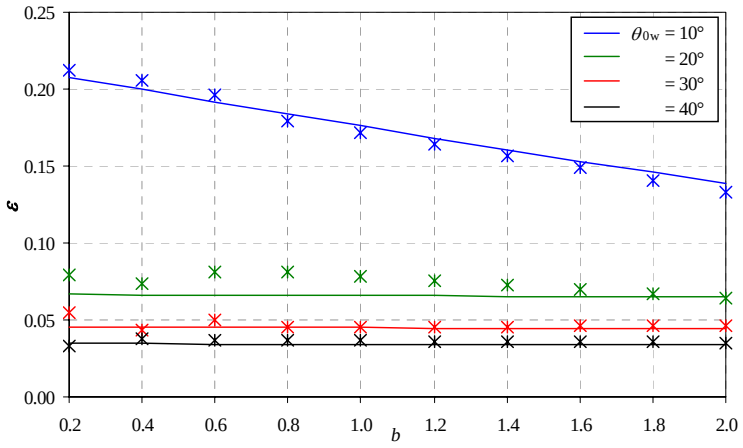

Fig. 5. Hyper-TSRB self-shading error versus scattering coefficient for $a = 0.02$ m^{-1}. Semi-analytical values (solid lines) were obtained with Eqs. (17) and (18) with $k_1 = 0.1$, and numerical results (asterisks) were computed with Backward Monte Carlo.

#5125 - $15.00 US Received 25 August 2004; revised 15 September 2004; accepted 16 September 2004
(C) 2004 OSA

Figure 6 shows the Hyper-TSRB self-shading error plotted versus total water depth (z_{bot}) as computed by the full analytical model of Eqs. (13) and (14). Values are for R_b = 0.2 and a = 0.2 m^{-1} and for several different sun positions. Note that the Hyper-TSRB upwelling radiance sensor is 0.66 m below the surface, so the distance from the sensor to the seafloor is (z_{bot} - 0.66). Also shown in Fig. 6 are Hyper-TSRB self-shading error results from Monte Carlo simulations for b/a = 2. In very shallow water the radiance measurement is dominated by the component of light being reflected off the seafloor. If the instrument is very close to the seafloor, it mostly sees its own shadow. As the water depth is increased (i.e., the instrument is moved further from the bottom), the shading error in the radiance reflected off the bottom decreases, as does the overall shading error. However, as the water depth is further increased, the water-column component of the upwelling radiance begins to dominate and the overall shading error increases toward the optically deep values. The existence of a shading minimum located a short distance from the seafloor has also been found to occur for upwelling irradiance sensors [15].

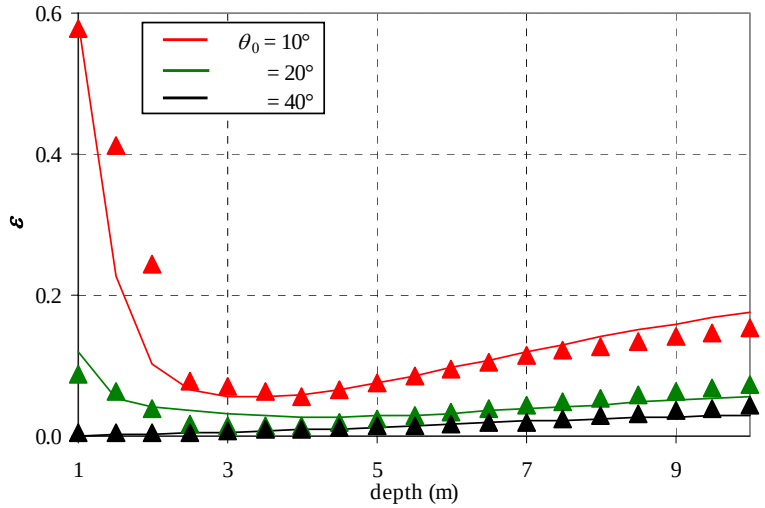

Fig. 6. Hyper-TSRB shading error as predicted with the analytical model compared with MC results (triangles). Results shown are for a = 0.2 m^{-1}, b = 0.4 m^{-1}, R_b = 0.2, FOV half-angle = 20º, and the indicated values of the solar zenith angle. The indicated depth is the total water depth; the sensor is 0.66 m below the sea surface.

The discrepancies in Fig. 6 between our analytical and numerical results at very small water depths is due primarily to the effects of internal reflection at the sea surface. When the water is very shallow, some of the sunlight experiences multiple reflections between the seafloor and the bottom of the sea surface, making the overall illumination on the instrument less collimated. This is taken fully into account in our Monte Carlo calculations, but not at all in the analytical results shown in Fig. 6. One can accommodate internal reflection in the analytical model in the same way that atmospheric scattering is accounted for [i.e., Eq. (15)]; however, this requires an estimate of the magnitude of the deviation of the in-water light from collimated.

4. Conclusions

Most commercially available instruments for measuring in-water upwelling radiance are large enough (i.e., with radii on the order of a few centimeters) that they suffer from significant self-shading error over at least some portion of the measured spectrum. The amount of error

#5125 - $15.00 US Received 25 August 2004; revised 15 September 2004; accepted 16 September 2004
(C) 2004 OSA

depends on instrument dimensions, water optical properties, sun position, and atmospheric conditions, and in optically shallow water also depends on sensor FOV, water depth, and seafloor optical properties. Because radiometer self-shading is minimal when the water absorption coefficient is small, there may be a tendency to ignore its effect in optically clear waters. However, even in the clearest of waters the magnitude of the absorption coefficient is greater than 0.2 m^{-1} for wavelengths $\lambda > 600$ nm and greater than 0.65 m^{-1} for $\lambda > 700$ nm [12], which gives deep-water Hyper-TSRB shading errors of $\varepsilon > 20\%$ and $\varepsilon > 50\%$, respectively, for $\theta_0 = 10^o$ and $\varepsilon > 5\%$ and $\varepsilon > 15\%$, respectively, for $\theta_0 = 30^o$ [Eq. (10)].

The self-shading error for unbuoyed radiometers in optically deep waters can be well estimated with the semianalytical model of Gordon and Ding [1]. We have provided analytical justification for this model and have extended it to include the effects of a buoy on instruments such as the Hyper-TSRB. We have also provided a semianalytical model for the Hyper-TSRB in deep water that takes scattering into account. For most practical purposes, however, the effects of scattering can be ignored in optically deep water.

It is important to note that the Gordon and Ding model cannot be applied in situations where the seafloor has a significant effect on the measured radiance. We have developed an analytical model for estimating the self-shading of a buoyed on unbuoyed radiometer close to the seafloor [Eqs. (11) and (12)] and linked it with the deep-water model with Eq. (13). It should be noted that the shallow-water and deep-water models do not bound the shading error; Eq. (13) may exhibit an minimum versus depth.

The error values provided Eqs. (10) and Eq. (11) are for a collimated light incident at a particular direction. To compute the overall error for particular illumination conditions, it is necessary to properly weigh the error values from all directions [e.g., Eq. (16)], and in very shallow water it may be necessary to take internal reflection at the sea surface into account.

In general, the self-shading error can be more accurately determined with Monte Carlo calculations than with an analytical model. However, the analytical approach is more general and is easier to disseminate and implement. The disadvantage of the numerical approach is that it requires a specialized computer code and that a large number of computations must be performed for each instrument. It is impractical to expect experimental oceanographers to write Monte Carlo codes for this purpose; however, it may the reasonable to expect instrument manufacturers to begin providing self-shading correction look-up tables or software with their products.

A great utility of the analytical model is its ability to predict the amount of shading that will be encountered while an experiment is in its planning stage. Experiments should be planned so as to best avoid the collection of upwelling radiance measurements at times when self-shading is greatest. For a given suite of instrumentation, only the time of deployment (e.g., the position of the sun) can be adjusted, but this may be sufficient. If an experiment cannot accommodate the time restrictions, then it may be necessary to invest in the development of smaller sensors or deployment packages for these experiments. The analytical model developed in this paper also provides a tool for instrument design; the effects of sensor-head radius, buoy radius, and buoy position on self-shading are all easily computed. Finally it should be noted that self-shading prediction and correction (by either analytical model or empirical data) requires considerable knowledge of the environment (e.g., water properties, water depth, bottom albedo, and atmospheric conditions). Our analytical model can be used to compute the sensitivity of self-shading to uncertainties in the environmental parameters given a particular instrument's dimensions.

Acknowledgments

This work was supported by the U. S. Office of Naval Research. We thank Howard Gordon for reviewing an early version of this document.

#5125 - $15.00 US Received 25 August 2004; revised 15 September 2004; accepted 16 September 2004
(C) 2004 OSA